International Journal of Engineering

Investigating the Effect of Clearance Distance between the Floor of a High-speed Train and Ground on Aerodynamic Forces in Presence of Side Wind

S. Norouzi[a], S. Hossainpour*[a], M. M. Rashidi[b]

[a] Department of Mechanical Engineering, Sahand University of Technology, Tabriz, Iran
[b] University of Electronic Science and Technology of China, Chengdu, 610054, Sichuan, PR China

P A P E R   I N F O

A B S T R A C T

The main objective of this paper was to propose the real model of the high speed train regarding the side wind disturbance. In the first part of this article, the turbulent air flow around a simplified design of a high-speed vehicle was numerically analyzed using finite volume method and four RANS turbulence models, including k-ω SST, k-ε RNG, Spalart-Almaras, and Launder and Sharma. The results of numerical simulations regarding the wall function were validated by experimental works and it was shown that in the area near the wall, the SST k-ω model had the best simulation for the horizontal component of the velocity (21% error). The results of the lift coefficients showed that at short distances from the train floor to the ground due to relatively strong wind with angles less than 0.2 radians, the lift coefficient was negative and as a result, the forces acting on the train were downward. Finally it was shown that by increasing the wind angle, this coefficient gradually becomes positive, which can disrupt the stability of the train. It can be concluded that in trains whose floor to ground distance is more than 0.136 of the train height, the balance is maintained only in the absence of side wind.

doi: 10.5829/ije.2023.36.04a.01

1. INTRODUCTION

The aerodynamic force on the train body, which is created as a result of changing the flow lines, is one of the most important design items. The flow around a train under normal conditions experiences a large-scale separation, which leads to large aerodynamic pressures and less stability. Aerodynamics of trains is a complex issue that needs to be considered for its accurate calculation. Among these things, we can optimize the shape of the train [1], the side wind effect [2-6], pressure changes when the train moves in the tunnel [7-9], the vortices at the end of the train [10], the flow passing under the train [11-13] and the impact of the ground on the air flow [14-17] are only some of the issues that researchers have addressed.

The effect of the ground on the flow around the train can be investigated from two aspects. The first effect is about the relative speed of the ground with the train and the second effect is about the distance between the floor of the train and the ground. Regarding the relative speed of the train with the ground in the experiments conducted using the wind tunnel, this effect is not considered in the results due to the fact that the ground is fixed in the wind tunnel. Zhang et al. [14] and Xia et al. [15] numerically studied the impact of fixed ground related to moving one. They observed that the boundary layer formed on the ground reduces the drag forces and excess the lift forces. Also, the assumption of a fixed ground increases the speed of flow slippage, which causes the formation of more open vortex structures and, as a result, vortex shedding with a higher frequency [18].

Far less research has been done on the effect of the distance of the floor of the train and the ground. Hajipour Khire Masjidi et al. [19] investigated the effect of the distance from the ground using a moving earth and a simple geometric shape (similar to the geometry that is examined in the first part of this article). Yu et al. [20]

*Corresponding Author Institutional Email: hossainpour@sut.ac.ir
(S. Hossainpour)

and Ismaiel [21] also used an aerodynamic shape to experimentally investigate the effect of distance from the ground on aerodynamic forces. According to their research, when the distance of the bottom of the device and the ground is reduced, the flow rejoins somewhere closer to the front of the model. Also, the lift force is clearly affected by this distance [22].

In today's high-speed trains, the distance between the floor of the train and the rail is very small. For example, one of the reasons for reducing the distance between the floor and the ground is installing panels to absorb noise on the rails [23]. In one of the few studies that was done to determine the effect of floor-to-ground distance on high-speed trains, Kalitzin et al. [24], for the first time, investigated the effect of this distance on the aerodynamic forces and flow field for the ICE3 high-speed train. Since they used the DES turbulence model for their numerical simulation, which is considered as a method with high computational cost, they had to use about 30 million computational cells, which is a very high computational cost in has found For this reason, they assumed the speed of the train to be 49.68 km/h, which is far from the speed of current high-speed trains. For this reason, in this article, firstly, the ability of RANS turbulence models to extract aerodynamic forces has been investigated, and then, using the best turbulence model, the air flow around the high-speed train at real speeds (250 km/h) has been investigated. It is simulated by using computing cells far less and the effect of the distance between the floor of the train and the ground on the aerodynamic forces at real speeds is investigated. Mahzoon and Kharati-Koopaee [25] have discussed the effects of the vehicle components and geometry in aerodynamic performance of the high speed trains. They have proposed the optimal length and windshield for the various longitudinal velocities, which can be used in sizing of the train considering its high speed in the design level.

In this article, first, to reach the best turbulence model for simulating the flow around an object, the flow around a rigid object is investigated and the velocity profile at different sections of the end region of the rigid object and the aerodynamic forces acting on it are compared with the experimental values. Despite the different studies done in the aerodynamic performance of the high speed ground vehicles, it seems that the separation area at the end of the bend remains a serious challenge for turbulence models, and there is a need to further examine these models in this area. According to the authors' information, in past studies, cumulative variables such as drag and drag coefficients were mostly calculated, and the amount of error resulting from these models in the reverse flow area has not been specifically studied. In this article, four commonly used models averaged in time with and without using wall functions are examined and the error rate of velocity profile estimation in the areas

near and far from the wall in the separation and return flow area is calculated and reported.

In the second part of this article, the geometry of the ICE3 high-speed train is designed as one of the newest high-speed trains in the world and is simulated using the best turbulence model in the first part of the article, the kwSST model. In this section, firstly, in order to ensure the design of the geometry and computational meshing operations, the simulation of the air flow around this high-speed train at a speed of 50 km/h and without the presence of side winds has been done. Then the profile of aerodynamic forces is compared with the available experimental data of this geometry. According to the authors' knowledge, no article has investigated the effect of side wind and the distance of the train floor from the ground on aerodynamic forces in high-speed trains. In the last stage of this article, the speed of the train has been increased to its actual value, i.e. 250 km/h, and the train has been exposed to side winds with different angles, and the impact of the distance of the train floor from the ground on the speed field and aerodynamic forces acting on the train in the presence of side wind have been investigated.

2. GEOMETRY OF MODEL

In this section, a simplified design of a vehicle is examined in three dimensions. The geometry of this model is designed in ICEM software. The geometry of this simplified model can be seen in 2D-3D in Figure 1.

2. 1. Governing Equations and Boundary Conditions   To simulate the flow passing over the vehicle in Figure 1, the equations of conservation of mass and momentum are used. Equations (1) and (2) represent the time-averaged mass and momentum equations (RANS) for an incompressible fluid in dimensionless form.
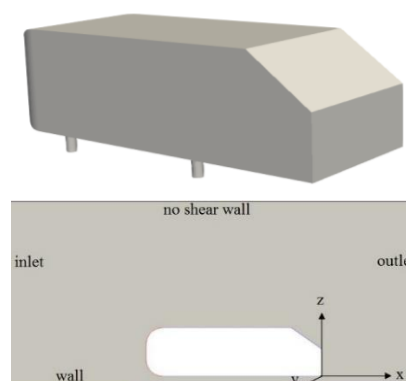
Figure 1. Model geometry: (a) front view; (b) back view (tilt angle 35 degrees); (c) Geometry of the vehicle from the side (inflow direction from left to right)

$$\frac{\partial \overline{u_i}}{\partial x_i} = 0 \tag{1}$$

$$\frac{\partial \overline{u_i}}{\partial t} + \frac{\partial \overline{u_i u_j}}{\partial x_j} = -\frac{\partial \overline{P}}{\partial x_i} + \frac{1}{Re}\frac{\partial}{\partial x_j}\frac{\partial \overline{u_i}}{\partial x_j} - \frac{\partial \tau_{ij}}{\partial x_j} \tag{2}$$

where $\overline{u_i}$ and $\overline{P}$ in these equations are the average values of velocity and pressure respectively, and $\tau_{ij} = \overline{u_i' u_j'}$ is the Reynolds stress tensor. In order to model the Reynolds stress term, many models have been presented so far. To select the best turbulence model, four important and widely used RANS models have been used in this research. These models include k-ω SST, k-ε RNG, Spalart-Almaras and Launder and Sharma. The last model is an improved low-Reynolds model based on k-ε. The Spallart-Almaras model is a one-equation model that has a lower computational cost than other models. All these models are used together with wall functions. Only the k-ω SST model has been implemented both with and without the wall function and the results were compared.

The boundary conditions of the problem are shown in Figure 1(c). The inlet boundary condition of speed equal to 40 m/s and the outlet boundary condition equal to zero constant pressure are considered. For the ground and the body of the vehicle, the condition of no slip and the upper surface of the wall without shear stress is considered.

2. 2. Numerical Method   In this research, the numerical analysis of the flow is done in the OpenFOAM and the simpleFOAM solver and steady solution are used. All terms of Navier-Stokes equations are discretized using second-order methods. The wall functions in the OpenFOAM open source code have been improved to provide acceptable results if the first cell is not exactly in the logarithmic region. The wall functions theory employed in OpenFOAM according to Kalitzin et al. [24]. In the topic of wall functions, the parameter y+, which is the dimensionless distance of the first center of the first calculation cell, is calculated from Equation (3):

$$y^+ = \frac{y u_\tau}{\nu} \tag{3}$$

where u_τ is the frictional velocity and y is the distance to the wall. uτ is calculated from Equation (4). As τw is the shear stress of the wall.

$$u_\tau = \sqrt{\frac{\tau_w}{\rho}} \tag{4}$$

Computational meshing has been done using the snappyHexMesh code, and important meshing parameters such as skewness, orthogonality, and aspect ratio have been considered as the general criteria of the computational mesh. In the wall nearby the mesh

accuracy was increased in 5 steps to properly present the velocity and pressure changes regarding the boundary conditions. For reducing the computational time and since we have used the medium size meshes, to increase of velocity and pressure accuracy near the rigid body, smaller meshes have been used in this part. Behind the train, there are flow vortices, positive pressure gradient and flow separation, which can only be correctly predicted with small sized meshes. Figure 2 depicts the side view of the computational grid near the rigid body on central plane.

3. RESULTS

3. 1. Grid Study   To check the independency of results from the grid size, the four grid sizes in Table 1 are used. The number of cells in these grids varies from about 2 millions to about 8 and a half millions.

Figure 3 shows the average horizontal and vertical velocity profile in a cross-section in the central plane of the domain (x=-0.023 m). As can be seen in this figure, as the number of cells increases, the accuracy of the solution gradually increases and the results converge to a single value. The results of Grid 3 are very close to the results of Grid 4 in most places. For this reason, Grid 3 is used in the rest of this article. Since number of computational cells are equal to 6 millions, near the walls y+>30, first computational cell is not located in area under the viscous layer.

3. 2. Investigating the Effect of Wall Function
The results of the velocity field at two different sections are shown in Figure 4 and compared with the empiricals.
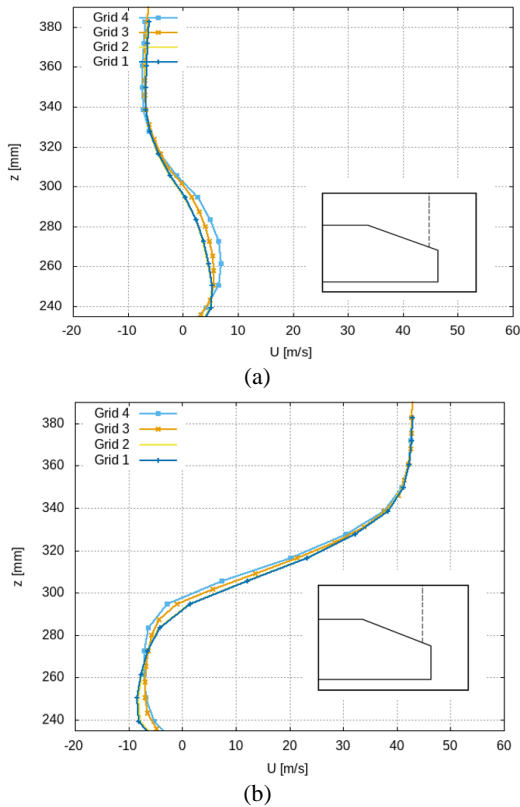
As shown in Figure 4, the use of the mentioned wall function reduces the computational cost and also increases the simulation accuracy near the wall. The
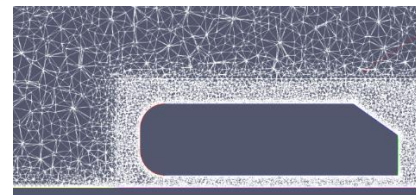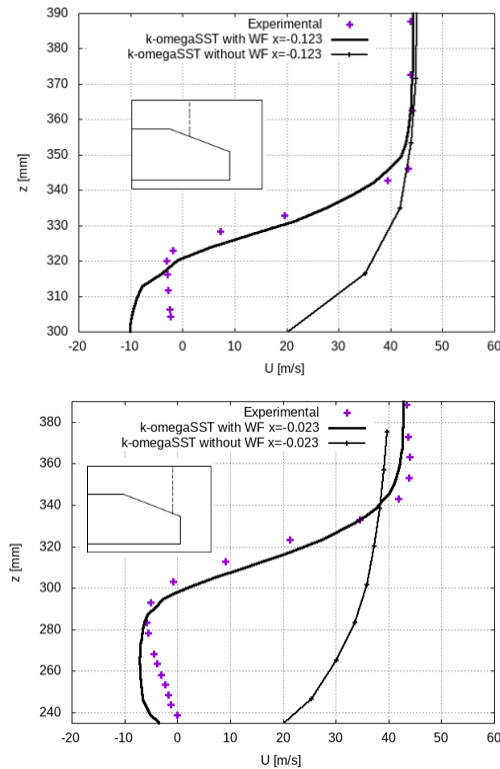

Figure 2. Computational grid side view for the near of rigid body

TABLE 1. Used computing networks

Number of cells	item
2200000	Grid 1
3700000	Grid 2
6600000	Grid 3
8500000	Grid 4

(a)

(b)

Figure 3. A) horizontal and B) vertical velocity profiles for four different computing grids in cross-section (x=-0.023 m)


Figure 4. The effect of using the wall function on the horizontal and vertical velocity profile for two vertical sections x=-0.023 and x=-0.123

results are close to each other at a distance far from the wall for both cases, while near the wall of the solid body where separation and flow reversal occur, the velocity profiles are very different from each other. As can be seen, the SST k-ω turbulence model using the wall function has provided relatively good results compared to the experimental values.

3. 3. Separation Area behind the Vehicle   Figure 5 depicts the profiles of horizontal (u) and vertical velocities (w) at several different vertical sections within (Figure 5) in the tail section using different turbulence models. As can be seen in these sections, near the wall to the height of the vehicle (about z=310 mm), the average horizontal velocity component is negative (backward flow) and the vertical velocity component of the air flow is positive (upward flow). This indicates the presence of positive gradient of pressure and return flow in this area.

As can be seen in Figure 5, the error rate of the turbulence models increases when approaching the wall of the vehicle, which is due to the presence of the wall effect and turbulent structures near the wall, as well as the presence of positive pressure and flow reversal, which is always considered as one of the main weaknesses of turbulence models. As can be seen in Figure 5, Lander and Sharma's one-equation model has the lowest and two models, k-ω SST, k-ε RNG, have the most agreement with the laboratory data.
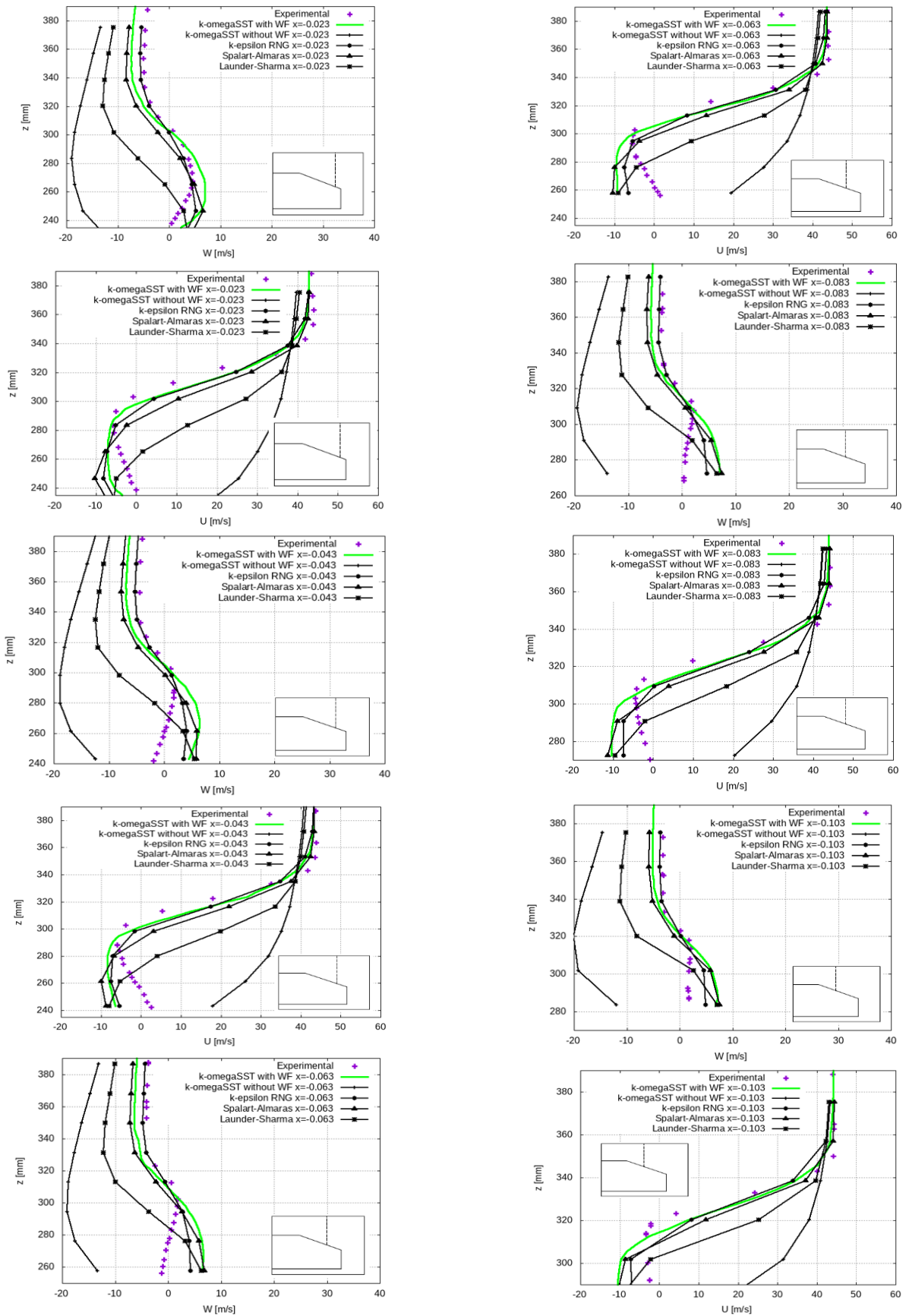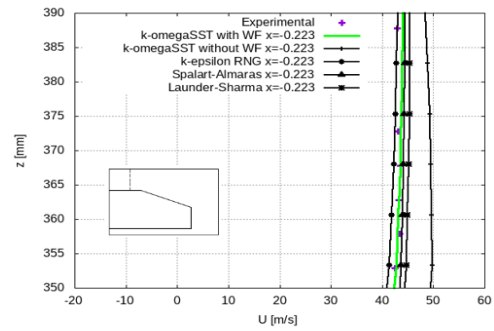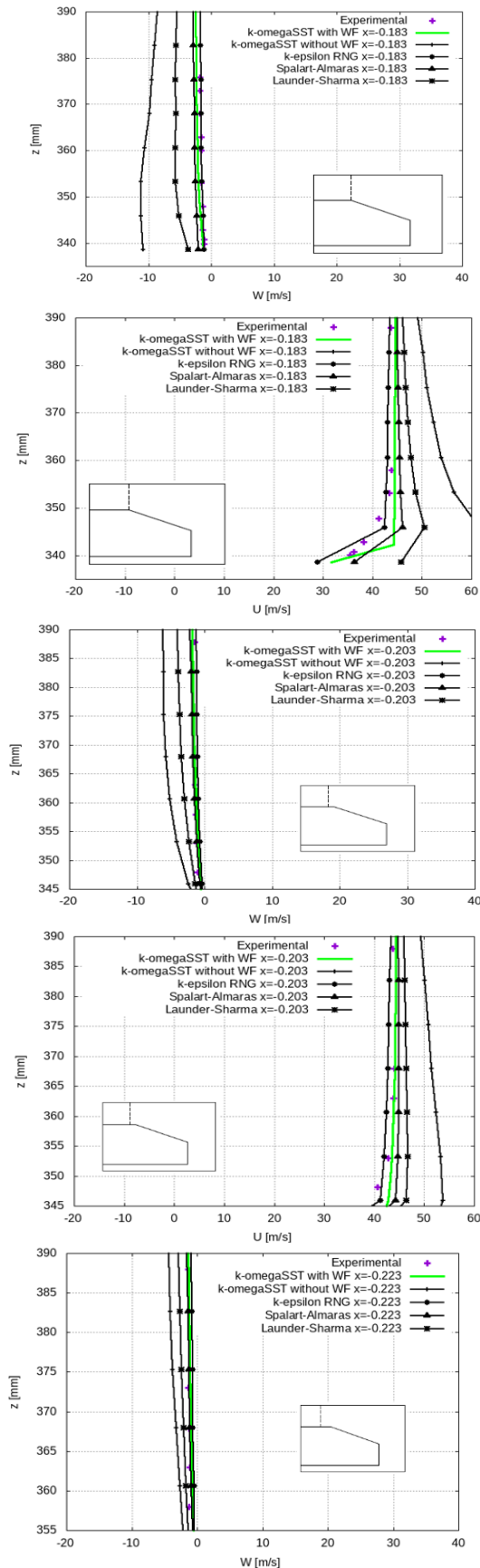
Figure 5. Variation of vertical and horizontal velocities in the tail section using different turbulence models

An important point that should be mentioned is the ability to estimate the average velocity field of these two models near the wall and (Z<310 mm) in the area far from the wall (Z>310 mm). In this research, the difference between the vertical and horizontal velocity profiles predicted by different turbulence models with experimental results was investigated for 10 different sections in the separation area behind the vehicle (the velocity profile of two sections is shown in this article). Table 2 summarized an average of the highest error percentage of different models in 10 different horizontal sections in the separation area.

As shown in Table 2, in the region near the wall (Z<310 mm), the SST k-ω model has the best simulation in the horizontal component of the average velocity field (21% error), while the RNG k-ε model, although it has shown a little more estimation error (24%), but the vertical component of the velocity has been estimated better in this area. On the other hand, the model has estimated the velocity field in the area slightly away from the wall with an error of 13% for the horizontal velocity field and 12% for the vertical velocity component, which is the best prediction compared to all models. The reason for this is the ability of this model to simulate the return flow and its separation.

3. 4. Investigating the Effect of the Distance between the Floor of the Train and the Ground on Aerodynamic Forces
In the current article, a resized 1:10 size of the ICE3 train was developed, which

TABLE 2. The average maximum relative error of different turbulence models in the separation region (compared to laboratory data) in percentage

Model	Z<310 mm		Z>310 mm	
	W	U	W	U
Launder and Sharma	230	405	110	210
Spalart Almaras	142	150	76	53
k-ω SST	35	21	20	15
k-ε RNG	29	24	12	13

contains 4 cabins whereas the length (L), width (W) and height (H) are respectively 10.14 meters, 29 0.0 m and 0.36 m (Figure 6). Previous studies by Mahzoon and Kharati-Koopaee [25] indicated that in high-speed trains, the impact of wheels on aerodynamic forces can be neglected, so in this study, their effect has been ignored. To investigate the effect of the distance of the floor of the train and the ground on the aerodynamic forces, 4 dimensionless distances from the floor of the train to the ground are considered as h/H=0.18, 0.136, 0.092, and 0.048.

For numerical simulations, the solution domain with the dimensions of 97W as the domain length, 20W as the domain height and 40W as the solution domain width has been used. The reason for using this large range is the lack of influence of boundary conditions on the flow structures around the train. In this section, flow fields and forces will be examined without considering side winds and considering side winds. Figure 7 shows the boundary conditions and solution domain in this case. The boundary conditions for the upper and side positions are considered symmetrically. To evaluate the relative speed of the train and the ground, the boundary condition of the ground is regarded as a wall with a speed equal to the free flow speed.

The beginning of the train is placed at a distance of 10W from the inlet boundary. The boundary condition at the outlet is considered to be fixed pressure and zero pressure. The distance of the train end to the exit boundary is equal to 52W, which is considered in order to check the vortex profiles behind the train and the lack of influence of the pressure boundary condition at the exit on the flow field at the end of the train. The speed at the inlet is assumed to be uniform on the entire surface of the inlet. In this case, based on the characteristic length (0.294 m = train height), flow speed (v=50 km/h), air density equal to 1.184 kg/m^3 and viscosity 1.855×10^{-5} kg/m s, Reynolds number is equal to Re=2.58×10^5 is considered. These specifications are mainly intended to match the previous experimental and numerical data and use them to verify the present work for the flow on the train without the influence of side winds [23]. In this article, to investigate the effect of the distance between the floor of the train and the ground (h in Figure 7) on the
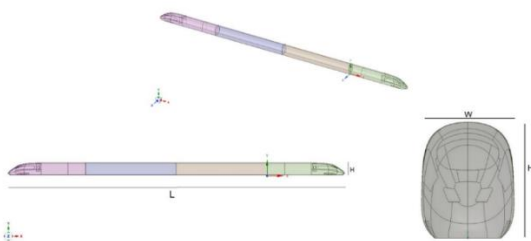
aerodynamic forces, 3 dimensionless distances (h/H)have been used, which are represented by symbols h0, h1 and h2, and the value of this the dimensionless distances are equal to 0.136, 0.092 and 0.048, respectively. The side wind speed (in the second part of this section) is equal to 20 km/h and is considered at 5 different angles.

The intended computational grid is done utilizing a grid with cubic organization for train geometry. This computational grid was made using GridPro software and then it was entered into the OpenFoam. Figure 8 shows the method of gridding on the surface of the ground and the surface of the ground near the ground.

Investigating more precisely the velocity and pressure fields, as well as to determine the eddies and turbulence flows created around and behind the train, the unstable URANS models and the k-w SST model have been used. In the entire implementation, the time step is determined as the CFL number which is shorter than 0.85. By this method, the time steps are determined in each time step, based on the simulation results in overall it is about 10^{-4} seconds in overall for time steps. Since the unsteady URANS models have been used, it is necessary to ensure sufficient solution time for the correct estimation of the mean flow parameters such as the mean speed and pressure. Figure 9 illustrates the drag coefficient value on the whole body from in duration time of 0-7 seconds, which is converged in time=5 s.

For checking the independence of the solution from the computational grid, 3 various grids used for the SST k-ω model (which was chosen in the previous section as the best model in predicting the flow fields around the rigid body). The explained grid strategy is the same for all three grids, but the number of cells in these three grids is 2 million, 4 million, 200 thousand and 8 million cells, respectively. Figures 10-a and 10b show the profile of the
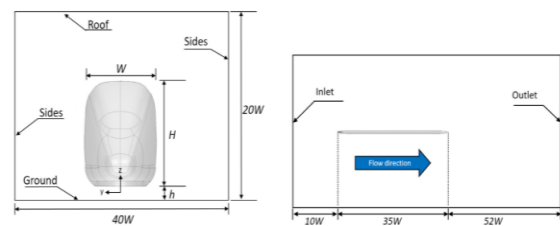
Figure 7. Solution domain and boundaries
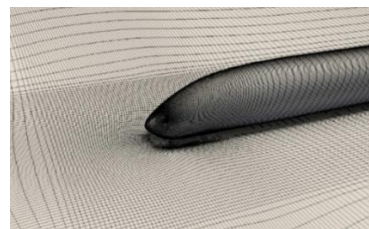
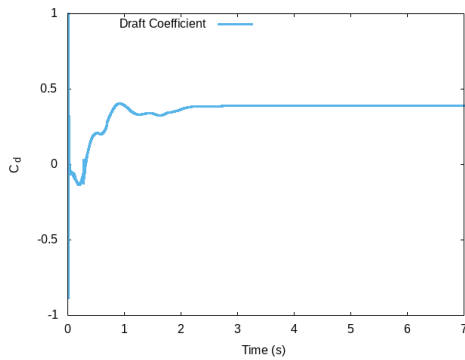**Figure 8.** Solution domain and boundary conditions

Figure 6. Trimetric, front and side views of the ICE3 high-speed train

Figure 9. Mean drag coefficient on the train

Figure 11. Simulation pressure coefficient comparison with previous experimental and numerical [18, 23]

horizontal and vertical velocity in the cross-section of the distance for the fixed longitudinal speed of 250 km/h. For the rest of the cases, the independence of the solution from the computational grid has been checked. As illustrated in Figure 10, the results for the various meshes are similar which approves the mesh indecency of the results. Therefore, in this research, a medium grid size with 4 million two hundred thousand cells has been used.

Figure 11 compares the simulation results with the laboratory findings of xia et al. [18] and Dong et al. [23]. Dong et al. [23] investigated the ICE3geometry. They simulated by employing LES and RANS hybrid turbulence method, utilizing IDDES method and Reynolds number similar to the present work. Xia et al. [18], studied the geometry of the ICE3 train without the
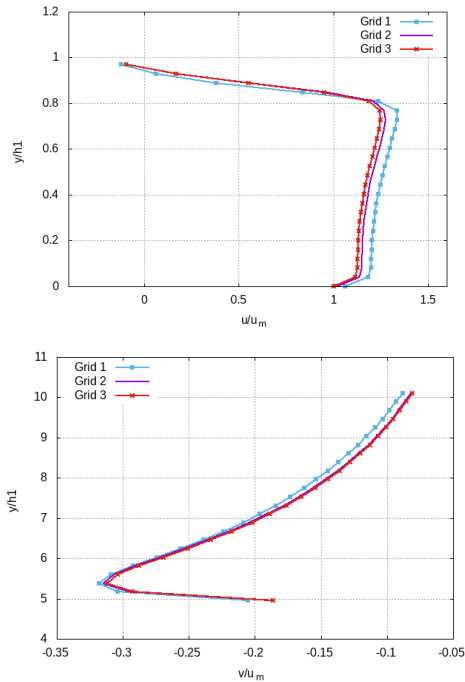
impact of side wind using a wind tunnel, but in their work, the Reynolds number was considered equal to 1.65 x 10^6, which is the same as the Reynolds number employed in the current research is different. Therefore, the laboratory data is slightly different from the simulation of Dong et al. [23] and also the present simulation.

3. 5. High Speed Train in the Presence of Crosswinds

3. 5. 1. Boundary Conditions   The boundary condition is considered exactly like the previous condition (Figure 7) with the difference that the left boundary is considered as the input boundary condition and the right boundary is considered as the output boundary condition.

3. 5. 2. Aerodynamic Forces and Moments
Figure 12 shows the speed diagram including wind speed w, train speed v and wind angle with respect to the direction of train movement β. In this article β is called yaw angle.

The relative speed of the wind to the speed of the train (u) is expressed as follows:

$$u^2 = v^2 + w^2 \tag{5}$$

And the yaw angle is defined as the following relationship.

$$\tan \beta = \frac{w}{v} \tag{6}$$

Figure 10. The effect of computational grid on the speed profile a) horizontal and b) vertical at different times

Figure 12. Velocity vector diagram
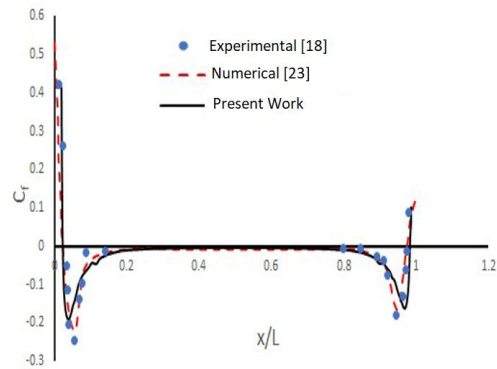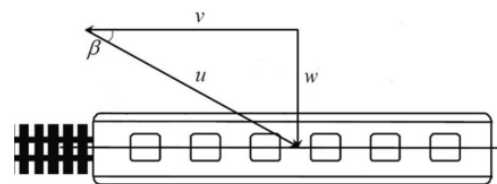
In the constant wind flow model, constant wind speed is considered. In this case, the aerodynamic forces are obtained from the following relations.

$$F = \frac{1}{2} \rho A C_F(\beta) u^2 \qquad (7)$$

where F is the aerodynamic force, C_F is the aerodynamic force coefficient, ρ is the air density, A is the reference area, and h is the reference height. In this section, the kωSST turbulence model is used in unsteady form.

3. 5. 3. Investigating the Impact of Train Floor Distance on Aerodynamic Forces at Various Yaw Angles

In this part, the effect of the distance of the train floor and the ground on the aerodynamic forces at various yaw angles will be investigated. For this purpose, 3 different distances from the floor to the ground h0, h1 and h2 are used and the speed of the wind flow is considered to be constant and equal to 20 m/s. All modes have been investigated for 6 different yaw angles from 0 to 0.5 radians (18 different modes in total).

Figure 13(a) shows the effect of floor to ground distance and yaw angle on the lift coefficient. As it can be seen, in all three distances, with an increase in the wind angle, the lift forces increase, so that for small distances (h1 and h2) in yaw angles less than 0.2 radians, the lift coefficient is negative, which means that the result of the vertical forces entering. It is downward on the train and therefore it causes the stability of the train in this direction. By increasing the direction of the wind to more than 0.2, the direction of the lift forces is changed and the lift coefficient is positive, which can cause the instability of the train at these angles.

For greater distances from the floor to the ground (h0), the lift coefficient is negative only in the absence of side wind, and when the side wind starts, the result of the lift forces is upward and causes the instability of the train. In this case, the maximum value of the lift coefficient is 1.43 at the yaw angle of 0.5.

Figure 13(b) shows the coefficient of side forces acting on the train due to side wind at different distances and angles. As can be seen, the lateral wind forces increase with the decrease of the distance between the train and the ground. The reason for this is the reduction of wind flow under the train. With the further increase of the wind angle and its passing over 0.4 radians, the
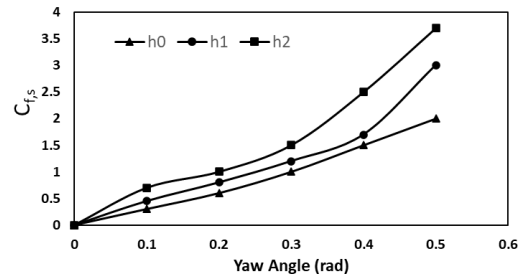

Figure 13. a) lift coefficient and b) drag coefficient related to the high-speed train in the presence of side winds with different angles and 3 different floor-to-ground distances

intensity of the increase in the side force increases, which can cause the stability of the train to be disturbed.

4. CONCLUSION

In this article, the influence of the height of the vehicle floor to the ground on the aerodynamic parameters in the presence of side wind flow was investigated. The presence of side wind had a great impact on stability and aerodynamic parameters, so considering its effect in the results, both in boundary conditions and in the analysis of aerodynamic forces, made the model more realistic. In this article, a detailed description of the selection of the turbulence model and its comparison with the previous valid references has been made on the bluff-body aerodynamics. In this article, using the OpenFOAM open source code, the air flow around a vehicle with a speed of 40 m/s (by considering the side wind) using four medium turbulence models taken at different times (in terms of the number of equations and also the working mechanism), including k-ω SST, k-ε RNG, Spalart-Almaras and Launder and Sharma with and without using the simulated wall function. The results indicate that Lander-Sharma and Spalart-Almaras models have very high errors (more than 400% for Lander-Sharma model) and these models are not capable of modeling the return flow. While the two models k-ω SST, k-ε RNG with the errors less than 25% can be considered as suitable options for checking the return flow. It was observed that the k-ω SST model has a better results in modeling the horizontal component of the velocity near the wall (the error is about 21%), while the k-ε RNG model better estimates the vertical part of the flow velocity as well as the flow velocity field in the area far from the wall.

5. REFERENCES

1. Krajnović, S., "Shape optimization of high-speed trains for improved aerodynamic performance", *Proceedings of the Institution of Mechanical Engineers, Part F: Journal of Rail*
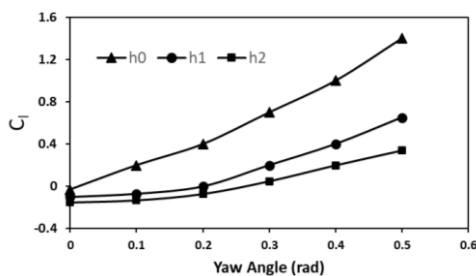
and Rapid Transit,   Vol. 223, No. 5, (2009), 439-452. https://doi.org/10.1243/09544097JRRT25

2. Webber, J., Mehbodniya, A., Teng, R., Arafa, A. and Alwakeel, A., "Finger-gesture recognition for visible light communication systems using machine learning", *Applied Sciences*, Vol. 11, No. 24, (2021), 11582. https://doi.org/10.3390/app112411582

3. Baker, C.J., Quinn, A., Sima, M., Hoefener, L. and Licciardello, R., "Full-scale measurement and analysis of train slipstreams and wakes. Part 1: Ensemble averages", *Proceedings of the Institution of Mechanical Engineers, Part F: Journal of Rail and Rapid Transit*, Vol. 228, No. 5, (2014), 451-467. https://doi.org/10.1177/0954409713485944

4. Zhang, L., Yang, M.-z. and Liang, X.-f., "Experimental study on the effect of wind angles on pressure distribution of train streamlined zone and train aerodynamic forces", *Journal of Wind Engineering and Industrial Aerodynamics*, Vol. 174, (2018), 330-343. https://doi.org/10.1016/j.jweia.2018.01.024

5. Adamu, A., Zhang, J., Gidado, F. and Wang, F., "An investigation of influence of windshield configuration and train length on high-speed train aerodynamic performance", *Journal of Applied Fluid Mechanics*,   Vol. 16, No. 2, (2022), 337-352. doi: 10.47176/jafm.16.02.1433.

6. Kargar, F., Mehdipour, R. and Baniamerian, Z., "A numerical investigation on aerodynamic coefficients of solar troughs considering terrain effects and vortex shedding", *International Journal of Engineering, Transactions C: Aspects*, Vol. 28, No. 6, (2015), 940-948. doi: 10.5829/idosi.ije.2015.28.06c.15.

7. Assadi, A. and Najaf, H., "Nonlinear static bending of single-crystalline circular nanoplates with cubic material anisotropy", *Archive of Applied Mechanics*, Vol. 90, No. 4, (2020), 847-868. https://doi.org/10.1007/s00419-019-01643-9

8. Najafi, M.L. and Nasiri, M., "Identification and prioritizing the effective factors on addiction by use of fuzzy analytical hierarchy process (f-AHP)", *Life Science Journal*, Vol. 10, No. 9s, (2013).

9. Chen, Z., Liu, T., Zhou, X. and Niu, J., "Impact of ambient wind on aerodynamic performance when two trains intersect inside a tunnel", *Journal of Wind Engineering and Industrial Aerodynamics*, Vol. 169, (2017), 139-155.

10. Rocchi, D., Tomasini, G., Schito, P. and Somaschini, C., "Wind effects induced by high speed train pass-by in open air", *Journal of Wind Engineering and Industrial Aerodynamics*, Vol. 173, (2018), 279-288. https://doi.org/10.1016/j.jweia.2017.10.020

11. Khosravian, E. and Maghsoudi, H., "Design of an intelligent controller for station keeping, attitude control, and path tracking of a quadrotor using recursive neural networks", *International Journal of Engineering, Transactions B: Applications*, Vol. 32, No. 5, (2019), 747-758. doi: 10.5829/ije.2019.32.05b.17.

12. Assadi, A., Najaf, H. and Nazemizadeh, M., "Size-dependent vibration of single-crystalline rectangular nanoplates with cubic anisotropy considering surface stress and nonlocal elasticity effects", *Thin-Walled Structures*, Vol. 170, (2022), 108518. https://doi.org/10.1016/j.tws.2021.108518

13. Paz, C., Suárez, E. and Gil, C., "Numerical methodology for evaluating the effect of sleepers in the underbody flow of a high-speed train", *Journal of Wind Engineering and Industrial Aerodynamics*,   Vol. 167, (2017), 140-147. https://doi.org/10.1016/j.jweia.2017.04.017

14. Zhang, J., Li, J.-j., Tian, H.-q., Gao, G.-j. and Sheridan, J., "Impact of ground and wheel boundary conditions on numerical simulation of the high-speed train aerodynamic performance", *Journal of Fluids and Structures*, Vol. 61, No., (2016), 249-261. doi. https://doi.org/10.1016/j.jfluidstructs.2015.10.006

15. Xia, C., Shan, X. and Yang, Z., "Comparison of different ground simulation systems on the flow around a high-speed train", *Proceedings of the Institution of Mechanical Engineers, Part F: Journal of Rail and Rapid Transit*, Vol. 231, No. 2, (2017), 135-147. https://doi.org/10.1177/0954409715626191

16. Wang, S., Burton, D., Herbst, A., Sheridan, J. and Thompson, M.C., "The effect of bogies on high-speed train slipstream and wake", *Journal of Fluids and Structures*, Vol. 83, (2018), 471-489. https://doi.org/10.1016/j.jfluidstructs.2018.03.013

17. Wang, S., Burton, D., Herbst, A.H., Sheridan, J. and Thompson, M.C., "The effect of the ground condition on high-speed train slipstream", *Journal of Wind Engineering and Industrial Aerodynamics*,   Vol. 172, (2018), 230-243. https://doi.org/10.1016/j.jweia.2017.11.009

18. Xia, C., Wang, H., Shan, X., Yang, Z. and Li, Q., "Effects of ground configurations on the slipstream and near wake of a high-speed train", *Journal of Wind Engineering and Industrial Aerodynamics*,   Vol. 168, (2017), 177-189. https://doi.org/10.1016/j.jweia.2017.06.005

19. Hajipour Khire Masjidi, B., Bahmani, S., Sharifi, F., Peivandi, M., Khosravani, M. and Hussein Mohammed, A., "Ct-ml: Diagnosis of breast cancer based on ultrasound images and time-dependent feature extraction methods using contourlet transformation and machine learning", *Computational Intelligence and Neuroscience*, Vol. 2022, (2022). doi: 10.1155/2022/1493847.

20. Yu, E., Jin, Y., Xu, G., Han, Y. and Li, Y., "Aerodynamic stability of typical sea-crossing bridge with streamlined box girder under wave-interfered complex wind fields", *Journal of Wind Engineering and Industrial Aerodynamics*, Vol. 228, (2022), 105101. https://doi.org/10.1016/j.jweia.2022.105101

21. Ismaiel, A., "Wind turbine blade dynamics simulation under the effect of atmospheric turbulence", *Emerging Science Journal*, Vol. 7, No. 1, (2022), 162-176. doi: 10.28991/ESJ-2023-07-01-012.

22. Zvolenský, P., Grenčík, J., Pultznerová, A. and Kašiar, Ľ., "Research of noise emission sources in railway transport and effective ways of their reduction", in MATEC Web of Conferences, EDP Sciences. Vol. 107, (2017), 00073.

23. Dong, T., Minelli, G., Wang, J., Liang, X. and Krajnović, S., "The effect of ground clearance on the aerodynamics of a generic high-speed train", *Journal of Fluids and Structures*, Vol. 95, (2020), 102990. https://doi.org/10.1016/j.jfluidstructs.2020.102990

24. Kalitzin, G., Medic, G., Iaccarino, G. and Durbin, P., "Near-wall behavior of rans turbulence models and implications for wall functions", *Journal of Computational Physics*, Vol. 204, No. 1, (2005), 265-291. https://doi.org/10.1016/j.jcp.2004.10.018

25. Mahzoon, M.M. and Kharati-Koopaee, M., "The effect of gurney flap and trailing-edge wedge on the aerodynamic behavior of an axial turbine blade", *HighTech and Innovation Journal*, Vol. 2, No. 4, (2021), 293-305. doi: 10.28991/HIJ-2021-02-04-03.

Persian Abstract

چکیده

هدف اصلی این مقاله ارائه مدل واقعی قطار سریع السیر همراه باد جانبی بود. در بخش اول این مقاله جریان هوای آشفته حول یک طرح ساده شده یک خودرو با سرعت بالا به صورت عددی با استفاده از روش حجم محدود و چهار مدل توربولانسی RANS شامل SST k-ω، k-ε RNG، Spalart-Almaras و Launder and Sharma و همچنین، تأثیر استفاده از تابع دیواره بر نتایج نیز بررسی شده است. نتایج شبیه‌سازی‌های عددی در رابطه با تابع دیوار با کارهای تجربی تأیید شد و نشان داد که در ناحیه نزدیک دیوار، مدل SST k-ω بهترین شبیه‌سازی را برای مؤلفه افقی سرعت (۲۱ درصد خطا) دارد. نتایج حاصل از لیفت نشان داد که در فواصل کوتاه از کف قطار تا زمین به دلیل وزش باد نسبتاً شدید با زوایای کمتر از ۰.۲ رادیان، ضریب لیفت منفی و در نتیجه نیروهای وارد بر قطار رو به پایین بوده است. در نهایت نشان داده شد که با افزایش زاویه باد، این ضریب به تدریج مثبت می شود که می تواند پایداری قطار را مختل کند. می توان نتیجه گرفت که در قطارهایی که فاصله کف آنها تا زمین بیش از ۰.۱۳۶ برابر ارتفاع قطار است، تعادل فقط در صورت عدم وجود باد جانبی حفظ می شود.